Iridescence in Metamorphic "Rainbow" Hematite

Xiayang Lin, Peter J. Heaney, and Jeffrey E. Post

The authors investigated "rainbow" hematite from Minas Gerais, Brazil, using electron microscopy, atomic force microscopy, and synchrotron X-ray diffraction to determine the cause of its intense wide-angle iridescence. The study revealed that the interference is produced by a highly periodic microstructure consisting of spindle-shaped hematite nanocrystals containing minor Al and P impurities. The nanorods are 200–300 nm in length and 50–60 nm in width. They are arranged in three orientations at 120° angles with respect to each other and stacked layer by layer to form the bulk crystal. The distances between adjacent parallel spindle-shaped particles within the same layer fall in the range of 280–400 nm, generating a diffraction grating for visible light. The organized substructure is apparent on all freshly fractured surfaces, suggesting that it represents more than an exterior surface coating. The authors propose that this periodic substructure results from arrested crystal growth by the oriented aggregation of hematite nanorods.

Hematite specimens that frequently display iridescence are described as "rainbow hematite" and "turgite" (figure 1). The latter term originated with the German mineralogist Rudolph Hermann, who coined it in 1844 to describe iron hydroxide specimens found near the Turginsk River in the Ural Mountains (Hermann, 1844). "Turgite" was discredited as a distinct mineral name in the 1920s, however, based on thermogravimetric (Posnjak and Merwin, 1919) and X-ray diffraction (Böhm, 1928; Palache et al., 1944) studies that identified such specimens as mixtures of microcrystalline hematite (Fe_2O_3) and either goethite (FeOOH) or amorphous Fe hydroxide. Nevertheless, "turgite" has been retained by the mineral collecting and gem community as a catch-all term for naturally iridescent iron (hydr)oxide minerals.

Mineral dealer Rock Currier (1940–2015) was largely responsible for introducing rainbow hematite to the U.S. market. According to notes he published on Mindat.org, Currier first visited an outcrop of what he called "color rock" from the Andrade mine in João Monlevade, Minas Gerais, Brazil, in 1991 (figure 2; Currier, 2012). Shortly after, he shipped a truckload of 55-gallon barrels filled with an estimated 15 tons of the material to the United States. Initially he attempted to sell the rainbow hematite "by the barrel for $3 per pound without very much luck." At a subsequent Tucson Gem and Mineral Show, however, he "arrived to find some guy had rented a big billboard and was selling the stuff as the latest and greatest metaphysical jewelry item. One guy was backing little pieces of the stuff with obsidian and selling earrings…for $90 a pair." Fortunately, Currier had kept enough of the rainbow hematite to select higher-grade samples, and he saw brisk sales of individual pieces.

Bulk samples of this Brazilian rainbow hematite are still sold at major mineral and gem shows, but our discussions with dealers indicate a growing

In Brief

- Iridescent hematite schists from Brazil were analyzed by high-resolution imaging and spectroscopy techniques.
- Rainbow colors arise from the interference of light waves reflecting off arrays of spindle-shaped hematite nanocrystals.
- These nanocrystals assembled through "oriented aggregation" as controlled by hematite's threefold symmetry.

See end of article for About the Authors and Acknowledgments.
Gems & Gemology, Vol. 54, No. 1, pp. 28–39,
http://dx.doi.org/10.5741/GEMS.54.1.28

Figure 1. Rainbow hematite from the Andrade mine in João Monlevade, Minas Gerais, Brazil. Photo © Rock Currier, Mindat.org.

scarcity. Currier attempted to purchase more material from the mine, but apparently the major seam of rainbow hematite at Andrade underlies the primary mine haul road, and excavation would have destabilized this conduit to the open pit. Nevertheless, exquisite pieces of rainbow hematite jewelry are still sold online, with accent stones such as amethyst, apatite, sapphire, tourmaline, and tsavorite (figure 3). Moreover, rainbow hematite plays an important role in the local culture. Villages neighboring the city of Belo Horizonte traditionally sprinkle the streets with truckloads of powdered material for festivals, creating an effect that Currier (2012) likened to "standing in a pile of peacock feathers."

To our knowledge, Ma and Rossman (2003a,b) have performed the only scientific investigation into the cause of iridescence in rainbow hematite, analyzing specimens from Brazil, Mexico, Italy, and several sites in the United States. Their results are also briefly highlighted in Nadin (2007). Using field-emission scanning electron microscopy (FESEM), Ma and Rossman (2003b) reported that their rainbow hematite specimens were coated with a "thin film" of rod-shaped nanocrystals, each measuring 5 to 35 nm in thickness and hundreds of nm in length. These nanocrystals were oriented in three directions, at 120º angles with respect to each other, and formed a grid-like network.

Figure 2. Rock Currier (left) and colleague survey a seam of rainbow hematite at the Andrade mine. Photo © Rock Currier, Mindat.org.

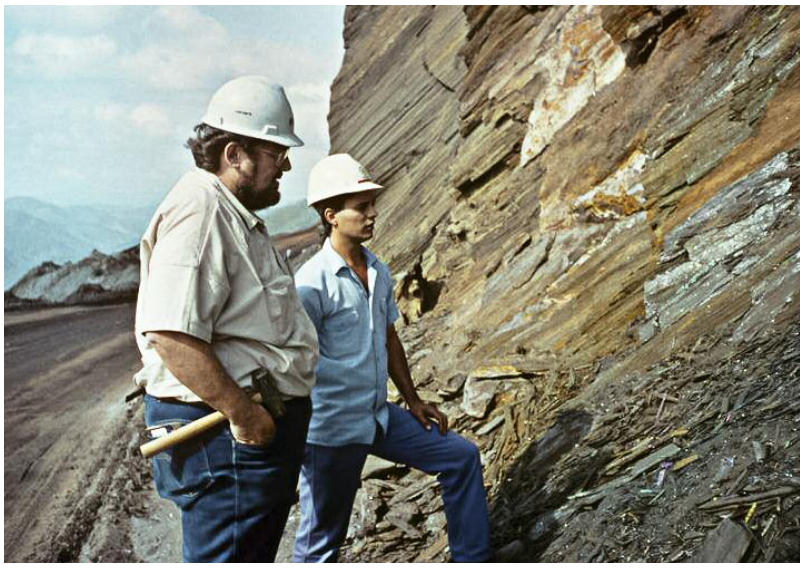

Figure 3. Left: An 18K gold pendant featuring rainbow hematite from Minas Gerais, Brazil, accented with amethyst and apatite. Right: Rainbow Rapture ring in 18K gold with tourmaline, sapphire, and tsavorite. Designs by Judith Anderson. Photos by The Jewelry Experts, Bijoux Extraordinaire, Ltd.

The nanocrystals were too small to determine precise chemical compositions, but energy-dispersive spectroscopy (EDS) revealed high concentrations of Al and P in a ratio that varied from 2.2 to 3.8. Ma and Rossman (2003b) noted that "the minute crystals have failed to produce either an X-ray powder diffraction pattern, an electron back-scatter diffraction pattern, or a Raman spectrum." The study interpreted the rod-like nanocrystals as a new mineral, but a full characterization was not possible with the resolution of the instrumentation.

Over the 15 years since these results were published online, more sophisticated analytical techniques have become available. For the present study, we sought to determine whether iridescence in rainbow hematite arises from thin-film effects involving Al phosphate phases, as earlier researchers hypothesized, or whether a different mechanism is involved. Rainbow effects in minerals are commonly attributed to nanoscale coatings, as in bornite (Buckley and Woods, 1983; Vaughan et al., 1987) and fire obsidian (Ma et al., 2001, 2007). Yet many gem materials (e.g., opal, labradorite, iris agate, and iris quartz) contain modular substructures that create a diffraction grating for visible light and generate rainbow effects (Darragh et al., 1966; Miura and Tomisako, 1978; Heaney and Davis, 1995; Lin and Heaney, 2017). These substructures often yield insights into exotic crystal growth processes that can inspire pathways for the self-assembly of synthetic materials. For the present investigation, we examined rainbow hematite from the Andrade mine using a combination of light optical microscopy, X-ray diffraction (XRD) and Rietveld analysis, FESEM, and atomic force microscopy (AFM).

MATERIALS AND METHODS

Specimen Description. We purchased the iridescent hematite samples used in this study at the 2014 Tucson Gem and Mineral Show from Cinderhill Gems (Meadow Vista, California), who traced the material to Rock Currier's bulk shipment from Brazil in the 1990s. The specimens we studied appeared identical in macroscopic physical character to those described by Currier (2012). As noted below, the microstructures matched the descriptions for Andrade hematite in Rosière et al. (2001) and Ma and Rossman (2003b). Thus, we concluded that the rainbow hematite in this study indeed derives from the Andrade mine.

The Andrade iron ore deposit is located in the eastern high-strain domain of the Quadrilátero Ferrífero district (figure 4) in the southern part of the São Francisco Craton of Brazil (de Almeida, 1977). The Quadrilátero Ferrífero (or "Iron Quadrangle") is so called because the Paleoproterozoic metasediments in the Minas Supergroup exhibit a rectangular arrangement of synclines (Rosière et al., 2001; Rosière and Chemale, 2008). The Caraça, Itabira, Piracicaba, and Sabará groups are four sequences of the Minas Supergroup rocks (Dorr, 1969; Mendes et al., 2017; see figure 5). The iron ore deposits are located within metamorphosed banded-iron formations in the Cauê Formation of the Itabira Group; the Andrade mine is in a contact-metamorphic zone within this formation. The rainbow hematite occurs as iridescent, specular seams oriented parallel to bedding. The material is brittle and fractures into lath-like splinters, but the crystals within the laths have a *granoblastic* texture, a term used to describe equigranular minerals without sharp crystal faces in metamorphic rocks. Rosière et al. (2001) attribute these textures to post-tectonic deformation and recrystallization.

The Andrade rainbow hematite seam occurs within a banded-iron formation (BIF) in the Itabira Group (again, see figure 5), which has lent its name to a broad class of metamorphic rocks called *itabirites*. These are hematitic (rather than mica) schists that formed when the original jasper bands in the BIF recrystallized into distinct layers of macroscopic quartz and hematite (or sometimes magnetite). The hematite schists, from which we infer the rainbow hematite derives, are intergrown within itabirites (Barbour, 1973).

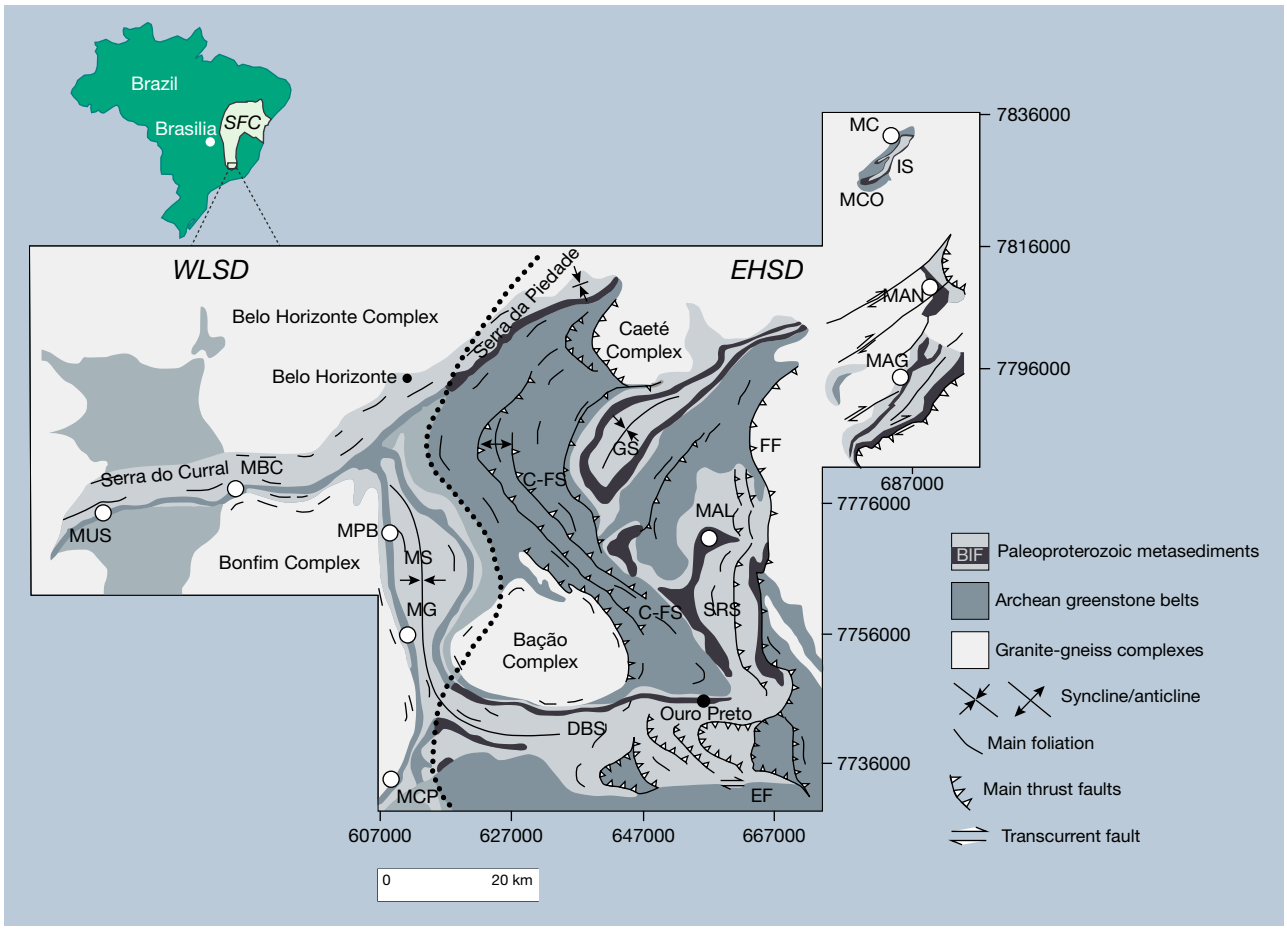

Figure 4. (A) Geologic map of the Quadrilátero Ferrífero in the southern portion of the São Francisco Craton (SFC), Brazil. Iridescent hematite derives from the Andrade mine, denoted toward the upper right as MAN. WLSD: Western Low-Strain Domain; EHSD: Eastern High-Strain Domain. IS: Itabira Syncline. From Mendes et al. (2017), as modified from Dorr (1969).

Scanning Electron Microscopy and Energy-Dispersive Spectroscopy. SEM and EDS were used to characterize surface topography and compositional information for the specimen. As iridescence was evident even from freshly fractured surfaces of the Andrade specimen, we removed a flake from one of our specimens and affixed the flake to an SEM mount using carbon fiber tape so that the flat iridescent surface was parallel to the surface of the SEM mount. We used an FEI Nova NanoSEM 600 field emission scanning electron microscope, outfitted with an Oxford Instruments X-Max (Model 51-XMX1105) silicon drift detector used for EDS analysis, in the Materials Characterization Laboratory (MCL) at Pennsylvania State University to examine the iridescent hematite. Nanoscale secondary electron images were obtained at an acceleration voltage of 5 kV and a current of 9 pA. EDS data were processed using the Oxford Instruments NanoAnalysis AZtec software (version 2.4). We chose three different accelerating voltages (20, 10, and 5 kV) to acquire spectra for the same sites.

Atomic Force Microscopy. To obtain high-resolution surface topography, we used a Bruker Icon I AFM (MCL, Pennsylvania State University) in PeakForce Tapping (PFT) mode with the ScanAsyst image optimization technique. In PFT mode, the cantilever is brought in and out of contact with the surface. PFT algorithms can precisely control the instantaneous force interaction, allowing the use of reduced forces in the imaging process. In this way, both fragile probes and samples can be protected without compromising image resolution. ScanAsyst automatically adjusts the appropriate parameters (such as set points, feedback grains, and scan rates) during the scan and continuously monitors image quality. The AFM probe for this analysis was a Bruker ScanAsyst-Air probe, which has a silicon tip on a nitride lever. The front angle of the

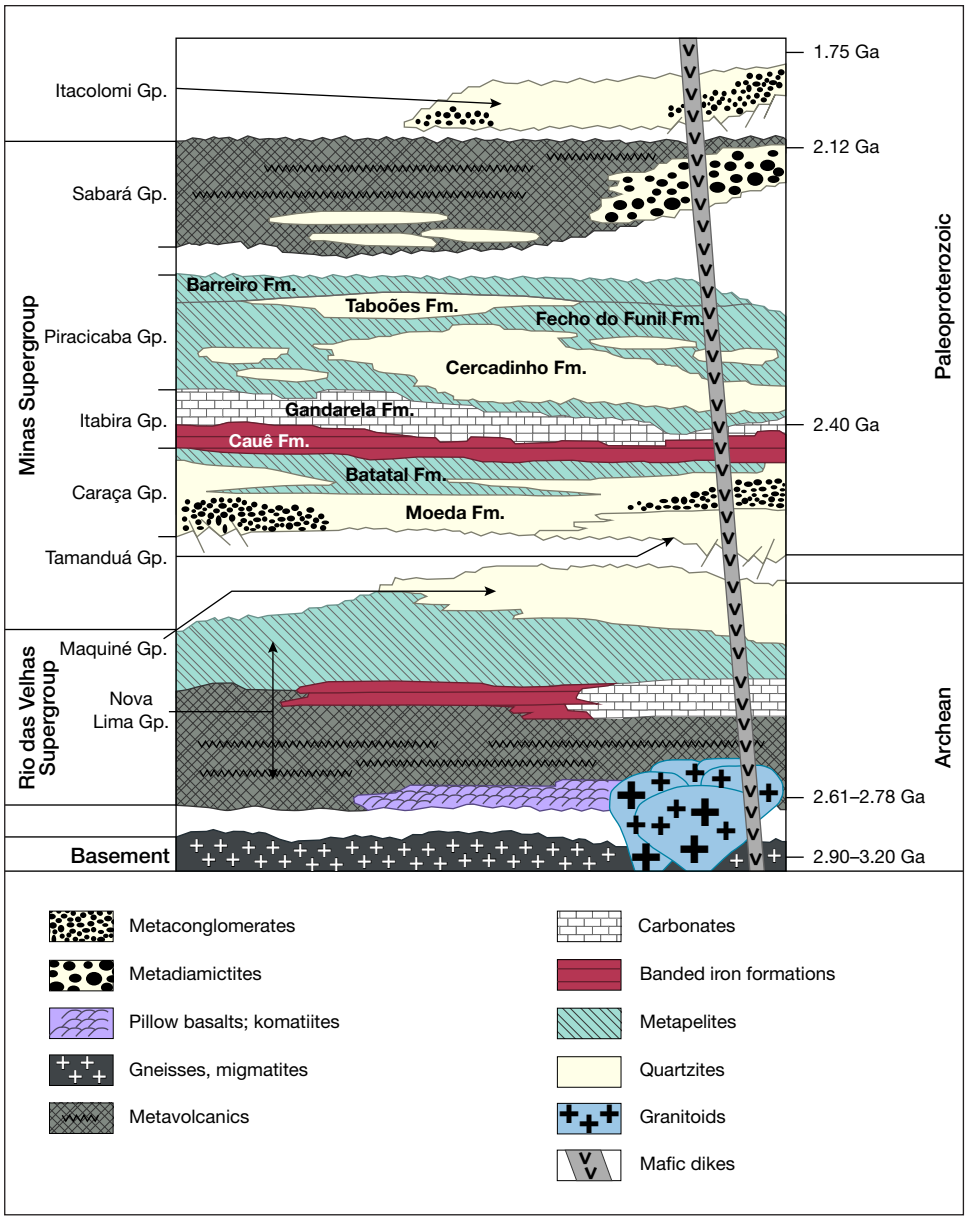

Figure 5. Stratigraphic column of the Quadrilátero Ferrífero. Rainbow hematite is found within the Cauê banded-iron formation. From Carlos et al. (2014).

tip was 15° and the back angle was 25°. For AFM imaging, the peak force set point ranged from 1 to 4 nN and the scan rate was 1 to 0.5 Hz, with 512 data points per line in each scan. NanoScope Analysis software (version 1.50) was used to process the AFM data.

X-Ray Diffraction. Hematite was powdered in an agate mortar and pestle under acetone. Upon drying, the powder was loaded into a 0.7 ID polyimide capillary for X-ray diffraction. Synchrotron X-ray diffraction data were collected at the GeoSoilEnviroCARS (GSECARS) 13-BM-C beamline at the Advanced Photon Source (APS), Argonne National Laboratory (Argonne, Illinois). The X-ray wavelength was 0.8315(4) Å, and the detector-sample distance was 100.469(1) mm. XRD data were collected with a MAR165 CCD camera. The diffraction pattern was integrated into intensity vs. 2θ plots using the Fit2D program with a polarization factor of 0.99 (Hammersley et al., 1996).

Structure Refinement. Rietveld refinement is a technique for determining atomic structures by comparing the misfit between an observed powder X-ray diffraction pattern and a diffraction pattern calculated on the basis of a model crystal structure (Rietveld, 1969). Factors such as unit-cell parameters and atom positions are allowed to refine until the misfit between the observed and calculated patterns

is minimized. Because we suspected that the atomic structure of the iridescent hematite from the Andrade mine might deviate from ideal hematite, we applied Rietveld analysis of the synchrotron XRD data to refine the crystal structure. The Rietveld software employed was the EXPGUI interface (Toby, 2001) of the general structure analysis system (GSAS) (Larson and Von Dreele, 1994). To obtain instrumental broadening parameters, we refined the structure of a LaB_6 standard using starting parameters from Ning and Flemming (2005). For the hematite refinement, we incorporated the peak profile parameters refined for LaB_6, and the initial structure parameters for hematite came from Blake et al. (1966). Using a 2θ range of 11.5° to 37.5° (d_{hkl} = 4.1 Å to 1.3 Å), we refined the background using a cosine Fourier series polynomial with eight profile terms. After the scale factor, background, unit-cell parameter, zero position, and additional profile terms had converged, the atom positions and the Fe occupancy were refined.

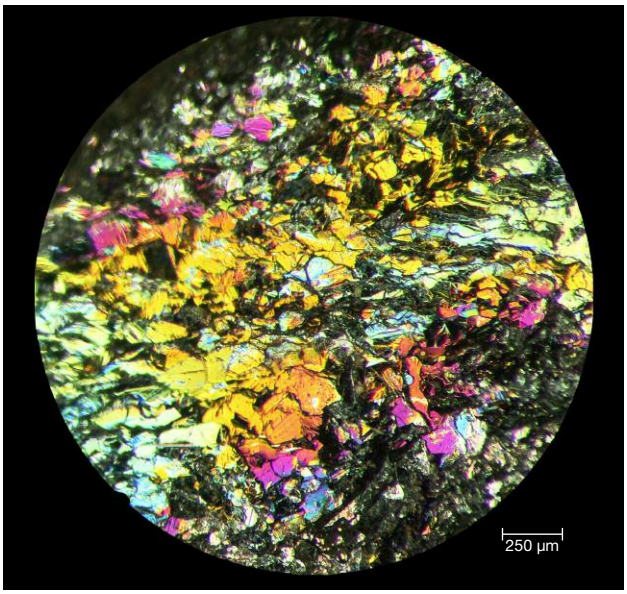

Figure 6. Reflected light microscope image of iridescent hematite revealing the granoblastic texture and strong iridescence of a freshly fractured surface. Photo by Xiayang Lin.

RESULTS

Reflected Light Microscopy. Viewed using reflected light optical microscopy at low magnification, the rainbow hematite sample appeared as a composite of gray hematite platelets with a strong silvery luster, and the platelets varied in diameter from 150 to 250 µm (figure 6). The lenticular to equidimensional texture was consistent with the mosaic granoblastic fabric reported by Rosière et al. (2001). Even when the iridescent Andrade hematite was freshly fractured, all surfaces exhibited intense rainbow colors (figure 6), leading us to interpret the iridescence as a bulk character, or at least as a pervasive character, rather than as the result of a single surface coating.

Scanning Electron Microscopy and Atomic Force Microscopy. When the iridescent surfaces of the Andrade hematite platelets from a freshly fractured surface were analyzed at low magnification using SEM, the surface appeared flat and smooth (figure 7). As first described by Ma and Rossman (2003a), however, sub-micron resolution revealed spindle- and rod-shaped nanocrystals arranged with threefold symmetry. The spindle-shaped particles were 200–300 nm in length and 50–60 nm in width. These oriented nanoparticles were reproducibly observable on freshly fractured surfaces, where they occurred as stacked sheets.

Figure 7. FESEM images of a freshly fractured iridescent hematite surface, shown with increasing magnification from left to right, reveal that the granoblastic texture of a single hematite grain (left) comprises individual nanocrystals oriented at 120° angles (center and right).

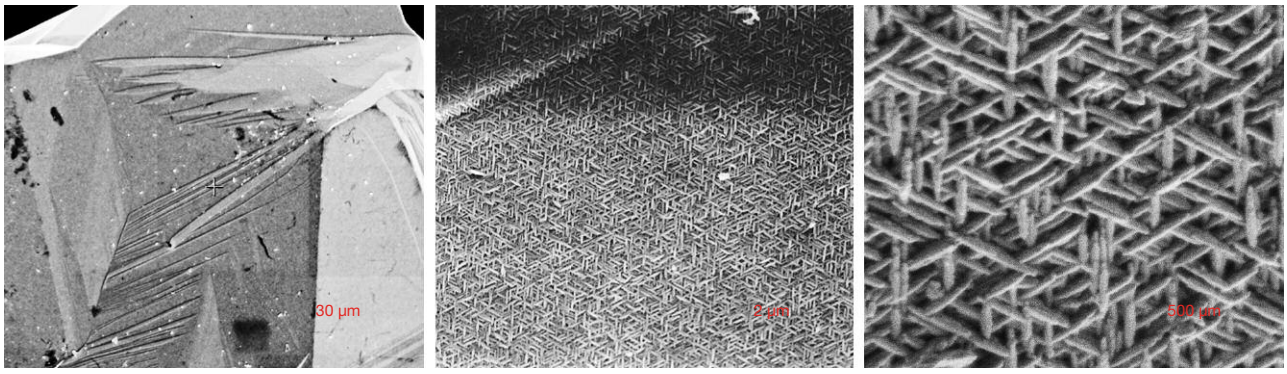

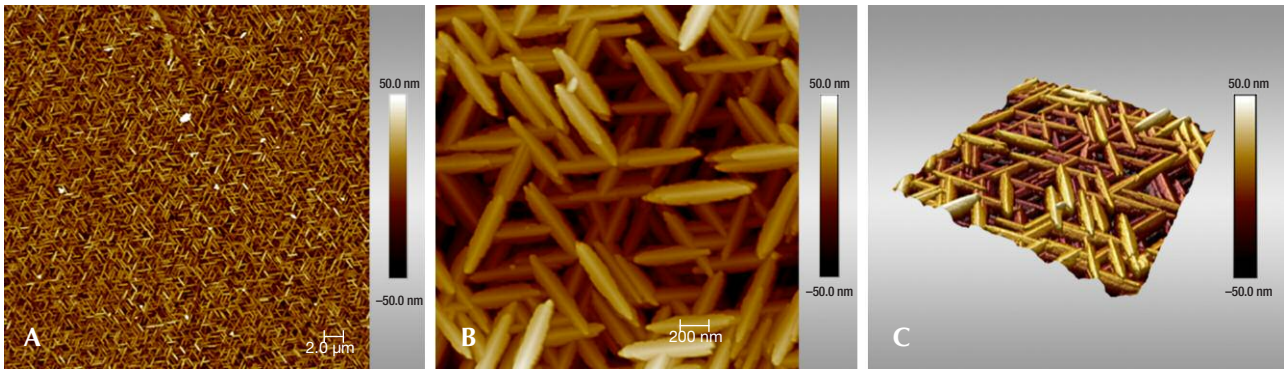

Figure 8. AFM images of iridescent hematite from the Andrade mine at low (A) and high (B) magnifications. The scale bar to the right of each image denotes the height relative to a zero-plane on the surface, with lighter colors representing higher elevations. (C) 3D reconstruction of the image in (B) as calculated by NanoScope Analysis software.

The threefold trellis network generated by the hematite nanoparticles was illustrated even more clearly by AFM imaging of fracture surfaces (figure 8). In particular, the scanning probe technique allowed for a three-dimensional reconstruction of the hematite surface (figure 8C), revealing a ridge-and-valley structure at the nanometer scale along three directions. Moreover, these images exposed a high concentration of nanopores approximately 10 nm in length.

Chemical Composition. We measured the elemental composition of the iridescent surface using EDS from a fractured face with nanoSEM (figure 9). Consistent with the results reported by Ma and Rossman (2003b), our EDS measurements detected Al and P in addition to Fe and O. Al is known to substitute for Fe in natural hematite (Tardy and Nahon, 1985; Cornell and Schwertmann, 2003, p. 51). Moreover, synthetic hematite with variable concentrations of substitutional Al has been studied extensively (Schwertmann et al., 1979; De Grave et al., 1985; Stanjek and Schwertmann, 1992; Gialanella et al., 2010; Liu et al., 2011). Likewise, P has been reported as a common impurity within natural hematite. Indeed, dephosphorization of iron ores to improve the efficiency of iron extraction is a global focus in the mining industry (Li et al., 2014; Lovel et al., 2015), including the Itabira deposits (Barbour, 1973). P-containing hematite also can be synthesized, and studies have revealed that P preferentially attaches to the prismatic (100) and (110) faces of hematite rather than the (001) and (104) basal faces (Colombo et al., 1994; Torrent et al., 1994; Gálvez et al., 1999), inducing particle morphologies to change from rhombohedral to spindle-shaped.

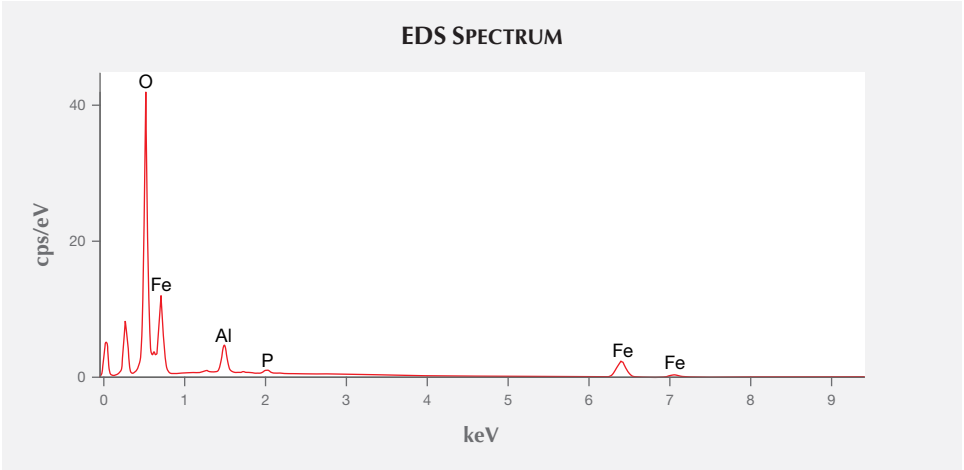

Figure 9. The EDS spectrum for iridescent hematite reveals the presence of Al and P in addition to Fe and O.

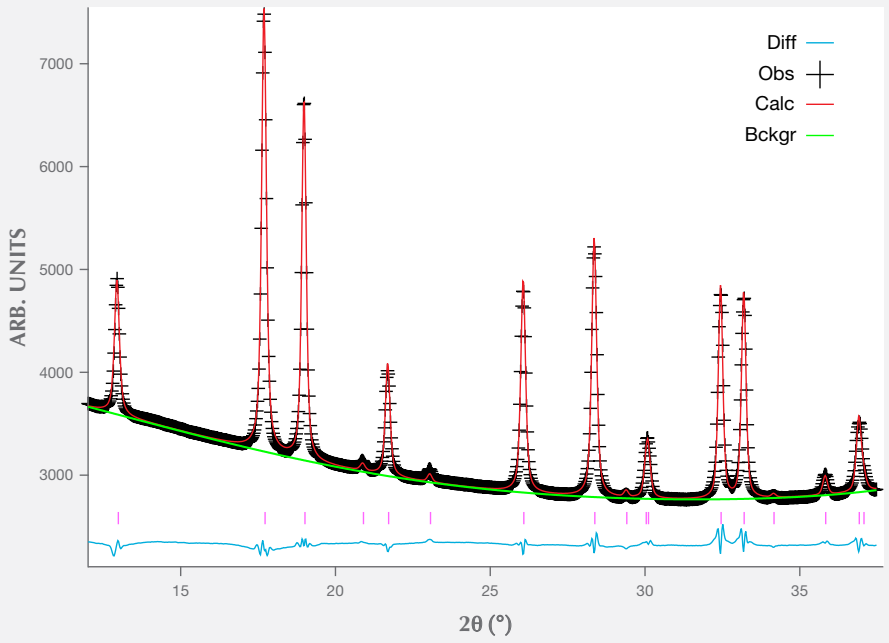

Figure 10. The close correspondence between the observed and calculated XRD patterns in this Rietveld refinement of iridescent hematite from the Andrade mine indicates a strong match between our model structure and the actual atomic structure. The black crosses represent the observed data. The red line is the calculated pattern based on the final refined structure. The green line models the background intensity. The blue line represents the difference between the observed and calculated patterns. The pink vertical lines mark the X-ray diffraction peaks of hematite.

Consequently, we calculated a formula for the iridescent hematite from the Andrade mine using the data in table 3 and assuming the presence of Al and P as impurities. Our EDS results yielded a formula of $Fe_{1.81}Al_{0.23}P_{0.03}O_3$, when normalized to three oxygen atoms. The absence of charge balance may indicate the P is not incorporated within the structure (see below), and it also may arise from the semi-quantitative nature of EDS when performed on a fractured rather than polished surface. Nevertheless, the ratio of Fe to Al suggests occupancies of 89% for Fe and 11% for Al, in good agreement with the results of our Rietveld analysis of XRD data, as described below.

XRD and Rietveld Refinement. Our X-ray diffraction analysis indicated that the Andrade mine hematites were phase pure within the detection limits of synchrotron diffraction (optimally about 0.1 wt.%). The final Rietveld refinement results based on our synchrotron XRD are presented in figure 10, and the unit-cell and refinement parameters are presented in table 1. Atom positions and occupancies are included in table 2.

Although the match between the calculated and observed patterns was excellent, we noted a discrepancy between our refined structure and ideal stoichiometric hematite. When we refined the structure using only Fe in the octahedral site, the occupancy converged to 93.9(4)% rather than 100%. Since our EDS results revealed the presence of Al, we postulated that Al was incorporated into the crystal structure of hematite rather than in the distinct phosphate phase suggested by Ma and Rossman (2003a). To test this hypothesis, we included Al on the same crystallographic site as Fe, with the constraint that the occupancies for Al and Fe would sum to 100%.

The accuracy of a Rietveld refinement is gauged using several goodness-of-fit (GOF) measurements. These include a factor that compares observed and calculated waveforms of the diffracted X-rays (R_{Bragg}) as well as factors that compare intensities of ob-

TABLE 1. Final Rietveld refinement parameters for iridescent hematite.

Space group	$R\bar{3}c$	Refinement parameters	
Unit cell		No. of diffraction points	1,062
a (Å)	5.0500(2)	No. of reflections	29
b (Å)	5.0500(2)	Diffraction range (2θ)	11.5–37.5
c (Å)	13.7903(6)	No. of variables	16
α (°)	90	$R(F^2)$	0.1136
β (°)	90	R_{WP}	0.0079
γ (°)	120	χ^2	0.2020

TABLE 2. Atomic coordinates and occupancy of iridescent hematite after Rietveld refinement.

Atom	*x*	*y*	*z*	Occupancy	U_{iso}
Fe	0	0	0.35530(6)	0.879(7)	0.004
Al	0	0	0.35530(6)	0.121(7)	0.004
O	0.2996(5)	0	0.25	1	0.004

served and calculated diffraction data as a function of scattering angle (χ^2 and R_{wp}). The partial substitution of Al for Fe improved the GOF by all of these measures, with R_{Bragg} decreasing from 0.1369 to 0.1136. Other GOF parameters indicated an excellent match between the calculated and observed diffraction patterns when Al substitution was allowed, with the final $\chi^2 = 0.2020$ and $R_{wp} = 0.0079$. Our final Rietveld refinement of the Andrade hematite yielded an occupancy for Fe of 87.9(7)%, with Al occupying the remaining 12.1(7)% of the sites. That value compares very well with the 11% occupancy for Al calculated from the EDS data.

Our efforts to incorporate P into the crystal structure did not yield a satisfactory structure refinement, which was not surprising since our EDS data suggested much lower concentrations of P than Al, consistent with the analyses of Ma and Rossman (2003b). Thus, P occurs as a minor impurity, either interstitially within the hematite structure, as a substitute for octahedral Fe, or perhaps as atoms attached to the surfaces of individual nanocrystals.

DISCUSSION

A Natural Diffraction Grating of Hematite Nanocrystals. Modulated structures with periodicities on the order of the wavelength of visible light (380–700 nm) can lead to diffraction effects if the structures are physically displaced relative to each other (such as ridges on a crystal surface) or if the nanostructure boundaries exhibit a change in refractive index (as with the alternating Na- and Ca-rich layers that characterize labradorite; reviewed in Lin and Heaney, 2017). Our observations indicate that the iridescence in metamorphic specular hematite from the Andrade mine results from the interference of visible light rays reflected from the stacked nanorods that constitute the bulk minerals. Consequently, the iridescence should not be attributed to a thin film of Al phosphate, as previously suggested by Ma and Rossman (2003a). Instead, the diffraction behavior is analogous to that generated by the modulated substructure in opal. Whereas opal consists of transparent, amorphous nanospheres that are closely packed to form a "photonic crystal" (Gaillou et al., 2008), the nanorods in iridescent hematite are crystalline, opaque, and primarily reflective of visible light.

The individual particles in the rainbow hematite were less than 100 nm wide, approaching the Rayleigh scattering domain (less than one-tenth the wavelength of light) and thus seemingly too small to diffract visible light. However, the average distances observed between parallel nanorods within the same layer were consistently in the range of 280–400 nm, the same order of magnitude as the wavelength of visible light. Consequently, the grating traced by the hematite nanoparticles was of a dimension suitable for scattering visible light.

Our inspection of many fragments of rainbow hematite revealed that the diffraction colors were independent of the angle of incidence. In other words, unlike play-of-color opal, which changes color as the sample is tilted with respect to the light source, the blue, green, and red patches of Andrade mine hematite did not change color as the specimens were rotated. This phenomenon is well known in biological materials with structural rather than pigmented coloration (e.g., the wings of the *Morpho* butterfly), and it appears to violate basic laws of light interference from periodic structures. For example, Bragg's law ($\lambda = 2d \sin \theta$) explicitly states that the wavelength of light (λ) is dependent on the spacing of the periodic substructure (d) and the incident light angle (θ). The apparent paradox embodied in this wide-angle diffraction behavior has been attributed to the combination of regular lamellar nanostructures (which create a strong interference effect) and irregular lamellar ridge heights (which diffuse the diffraction) (Kinoshita et al., 2002; Song et al., 2014). The hematitic substructures seen in figure 8C reveal regular lamellar features with variable topography, perhaps accounting for the angle-independent iridescence.

TABLE 3. EDS analysis using elemental *K*-lines for iridescent hematite.

Element	Wt.%	Wt.% sigma	Atomic %
O	30.78	0.21	59.23 ± 0.2
Al	4.01	0.06	4.58 ± 0.1
P	0.54	0.04	0.54 ± 0.1
Fe	64.67	0.24	35.65 ± 0.2
Total	100		100

Ordered Substructures from Oriented Aggregation. The periodic substructure of specular hematite from the Andrade mine consists of nanorods oriented at 120° angles with respect to each other and stacked layer by layer. This texture strongly suggests crystal growth by oriented aggregation of nanohematite (Niederberger and Cölfen, 2006). In this crystal growth mechanism, individual primary crystallites nucleate and grow to a specific length, followed by the assembly of mineral grains in a crystallographically controlled fashion (Penn and Banfield, 1998; Banfield et al., 2000). Hematite has a particular tendency to form through aggregation-based processes. Oriented aggregation of pseudocubic, ellipsoidal, and disc-shaped crystals has been described in a variety of hematite synthesis studies (Sugimoto et al., 1993; Ocaña et al., 1995; Niederberger et al., 2002).

We propose that the iridescent hematite found at the Andrade mine formed in two stages (figure 11). During the first stage, ultrafine crystallites grew as spindle-shaped rather than rhombohedral nanoparticles. The rod-like morphology may have resulted from the incorporation of Al and/or P within the crystal structure (Schwertmann et al., 1979; Barron et al., 1988; Reeves and Mann, 1991; Stanjek and Schwertmann, 1992; Sugimoto et al., 1993, 1998; Colombo et al., 1994; Galvez et al., 1999). It has been suggested that these ions poison surface sites and induce the growth of non-equant crystals.

In the second stage of growth, the nanorods assembled such that their crystallographic c-axes were parallel. Because hematite has trigonal (threefold) symmetry along the c-axis, two crystals can align in one of three orientations with equivalent energetics of attachment (energy of structural assembly), giving rise to the threefold rotational orientations seen in figures 7 and 8. This interpretation suggests that the particles are elongated perpendicular to the c-axis, in contrast to an earlier finding that ellipsoidal hematite is lengthened along the c-axis (Colombo et al., 1994). Whereas most crystals that form by oriented aggregation eventually fill all spaces, the iridescent hematite from the Andrade mine records an arrested growth, with significant retention of void space. Researchers have attributed the occurrence of hematite in the Cauê Formation to the hydrothermal recrystallization of magnetite (Rosière and Rios, 2004). The density of hematite (5.26 gm/cm^3) is greater than that of magnetite (5.18 gm/cm^3). Thus, the replacement of magnetite by hematite will generate porosity if the volume of the rock unit is unchanged (Putnis, 2002).

Ma and Rossman (2003a) deserve credit for their initial SEM observations of the periodic surface textures, and their online images reveal very similar microstructures in specimens from other localities.

Figure 11. Our model for the formation of the texture observed in iridescent hematite from the Andrade mine. Rod-like nanocrystals of hematite grow to a critical size and population density before assembling with crystallographic control to generate the threefold trellis network observed.

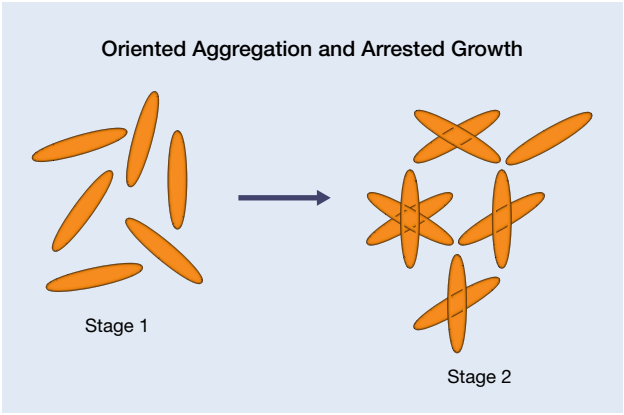

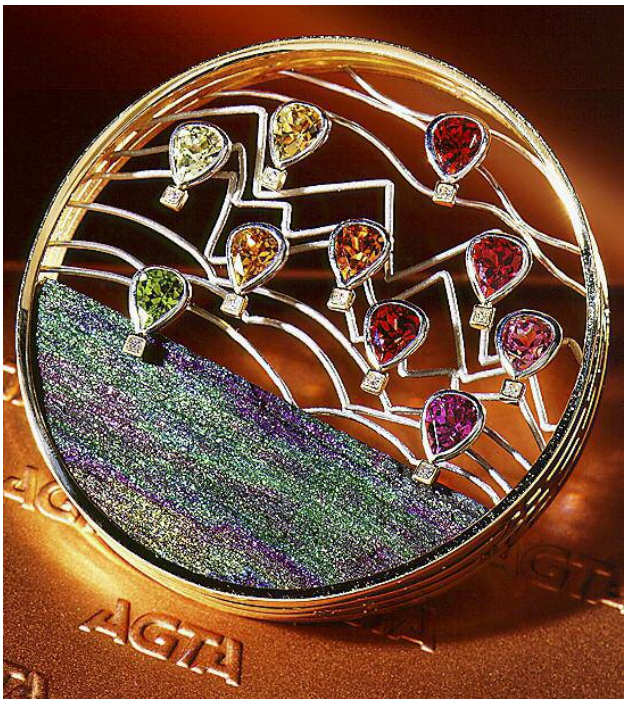

Figure 12. "Flying Free," designed by Llyn Strelau, features Brazilian rainbow hematite and mixed colored garnets set in yellow gold and platinum. The brooch received an AGTA Spectrum Award in 1995. Photo courtesy of Jewels by Design.

In particular, iridescent hematite specimens from the El Salvador mine in Mexico (labeled GRR 1960), Quartz Mountain, Oregon (GRR 2380), and Alaska (CIT 11952) exhibit stacked, oriented aggregates of what we propose are hematite nanocrystals. We conclude that the hydrothermal recrystallization of precursor magnetite, which commonly occurs when banded-iron formations are metamorphosed, may favor porous hematite with crystallographically oriented nanocrystals, giving rise to iridescent specular hematite (figure 12) in many localities around the world.

ABOUT THE AUTHORS

Ms. Lin received her M.S. in geosciences at Pennsylvania State University in 2015. After two years with the Rapaport Diamond Corporation, she is starting her own gem trading firm in China. Dr. Heaney is a professor in the Department of Geosciences at Pennsylvania State University. Dr. Post is the curator of the National Gem and Mineral Collection in the National Museum of Natural History, Smithsonian Institution, in Washington, DC.

ACKNOWLEDGMENTS

This research was made possible through funding from the National Science Foundation (NSF-EAR11-47728 and EAR-1552211). SEM and AFM work were performed at the Materials Characterization Laboratory at Pennsylvania State University with the assistance of Dr. Trevor Clark, Julie Anderson, Joshua Maier, and Timothy Tighe. Special thanks are due to Drs. James Kubicki, Maureen Feineman, and Phil Kong for their useful suggestions and assistance.

REFERENCES

de Almeida F.F.M. (1977) O cráton do São Francisco. *Brazilian Journal of Geology*, Vol. 7, No. 4, pp. 349–364.

Banfield J.F., Welch S.A., Zhang H., Ebert T.T., Penn R.L. (2000) Aggregation-based crystal growth and microstructure development in natural iron oxyhydroxide biomineralization products. *Science*, Vol. 289, No. 5480, pp. 751–754, http://dx.doi.org/10.1126/science.289.5480.751

Barbour A.P. (1973) Distribution of phosphorus in the iron ore deposits of Itabira, Minas Gerais, Brazil. *Economic Geology*, Vol. 68, No. 1, pp. 52–64, http://dx.doi.org/10.2113/gsecongeo.68.1.52

Barron V., Herruzo M., Torrent J. (1988) Phosphate adsorption by aluminous hematites of different shapes. *Soil Science Society of America Journal*, Vol. 52, No. 3, pp. 647–651, http://dx.doi.org/10.2136/sssaj1988.03615995005200030009x

Blake R.L., Hessevick R.E., Zoltai T., Finger L.W. (1966) Refinement of the hematite structure. *American Mineralogist*, Vol. 51, No. 1-2, pp. 123–129.

Böhm J. (1928) Röntgenographische Untersuchung der mikrokristallinen Eisenhydroxydminerale. *Zeitschrift für Kristallographie*, Vol. 68, No. 1-6, pp. 567–585, http://dx.doi.org/10.1524/zkri.1928.68.1.567

Buckley A.N., Woods R. (1983) X-ray photoelectron spectroscopic investigation of the tarnishing of bornite. *Australian Journal of Chemistry*, Vol. 36, No. 9, pp. 1793–1804, http://dx.doi.org/10.1071/CH9831793

Carlos D.U., Uieda L., Barbosa V.C.F. (2014) Imaging iron ore from the Quadrilátero Ferrífero (Brazil) using geophysical inversion and drill hole data. *Ore Geology Reviews*, Vol. 61, pp. 268–285, http://dx.doi.org/10.1016/j.oregeorev.2014.02.011

Colombo C., Barrón V., Torrent J. (1994) Phosphate adsorption and desorption in relation to morphology and crystal properties of synthetic hematites. *Geochimica et Cosmochimica Acta*, Vol. 58, No. 4, pp. 1261–1269, http://dx.doi.org/10.1016/0016-7037(94)90380-8

Cornell R.M., Schwertmann U. (2003) *The Iron Oxides: Structure, Properties, Reactions, Occurrences and Uses*. John Wiley & Sons, New York.

Currier R. (2012) A story about color rock. Mindat.org, https://www.mindat.org/article.php/1481//A+story+about+color+rock

Darragh P.J., Gaskin A.J., Terrell B.C., Sanders J.V. (1966) Origin of precious opal. *Nature*, Vol. 209, No. 5018, pp. 13–16, http://dx.doi.org/10.1038/209013a0

De Grave E., Verbeeck A.E., Chambaere D.G. (1985) Influence of small aluminum substitutions on the hematite lattice. *Physics Letters A*, Vol. 107, No. 4, pp. 181–184, http://dx.doi.org/10.1016/0375-9601(85)90837-0

Dorr J.V.N. (1969) Physiographic, stratigraphic, and structural development of the Quadrilátero Ferrífero, Minas Gerais, Brazil. *U.S. Geological Survey Professional Paper*, No. 641-A.

Gaillou E., Fritsch E., Aguilar-Reyes B., Rondeau B., Post J., Barreau A., Ostrooumov M. (2008) Common gem opal: An investigation of micro-to nano-structure. *American Mineralogist*, Vol. 93, No. 11-12, pp. 1865–1873. https://doi.org/10.2138/am.2008.2518

Gálvez N., Barrón V., Torrent J. (1999) Preparation and properties of hematite with structural phosphorus. *Clays and Clay Minerals*, Vol. 47, No. 3, pp. 375–385, http://dx.doi.org/10.1346/CCMN.1999.0470314

Gialanella S., Girardi F., Ischia G., Lonardelli I., Mattarelli M., Montagna M. (2010) On the goethite to hematite phase transformation. *Journal of Thermal Analysis and Calorimetry*, Vol. 102, No. 3, pp. 867–873, http://dx.doi.org/10.1007/s10973-010-0756-2

Hammersley A.P., Svensson S.O., Hanfland M., Fitch A.N., Hausermann D. (1996) Two-dimensional detector software: From real detector to idealised image or two-theta scan. *High Pressure Research*, Vol. 14, No. 4-6, pp. 235–248, http://dx.doi.org/10.1080/08957959608201408

Heaney P.J., Davis A.M. (1995) Observation and origin of self-organized textures in agates. *Science*, Vol. 269, No. 5230, pp. 1562–1565, http://dx.doi.org/10.1126/science.269.5230.1562

Hermann R. (1844) Untersuchungen russischer Mineralien. *Journal für Praktische Chemie*, Vol. 33, No. 1, pp. 282–300, http://dx.doi.org/10.1002/prac.18440330139

Kinoshita S., Yoshioka S., Kawagoe K. (2002) Mechanisms of structural colour in the *Morpho* butterfly: Cooperation of regularity and irregularity in an iridescent scale. *Proceedings of the Royal Society of London B: Biological Sciences*, Vol. 269, No. 1499, pp. 1417–1421, http://dx.doi.org/10.1098/rspb.2002.2019

Larson A.C., Von Dreele R.B. (1994) GSAS: General Structure Analysis System. *Los Alamos National Laboratory Report*, LAUR 86-748.

Li Y., Sun T., Kou J., Guo Q., Xu C. (2014) Study on phosphorus removal of high-phosphorus oolitic hematite by coal-based direct reduction and magnetic separation. *Mineral Processing and Extractive Metallurgy Review*, Vol. 35, No. 1, pp. 66–73, http://dx.doi.org/10.1080/08827508.2012.723648

Lin X., Heaney P.J. (2017) Causes of iridescence in natural quartz. *G&G*, Vol. 53, No. 1, pp. 68–81, http://dx.doi.org/10.5741/GEMS.53.1.68

Liu Q.S., Torrent J., Barrón V., Duan Z.Q., Bloemendal J. (2011) Quantification of hematite from the visible diffuse reflectance spectrum: effects of aluminium substitution and grain morphology. *Clay Minerals*, Vol. 46, No. 1, pp. 137–147, http://dx.doi.org/10.1180/claymin.2011.046.1.137

Lovel R.R., Sparrow G.J., Fisher-White M.J. (2015) Developments in chemical separation of iron ore. In L. Lu, Ed., *Iron Ore: Mineralogy, Processing and Environmental Sustainability*, Woodhead, Amsterdam, pp. 357–372.

Ma C., Rossman G. (2003a) Low voltage FESEM of geological materials. *Microscopy and Microanalysis*, Vol. 9, No. S2, pp. 990–991.

Ma C., Rossman G.R. (2003b) Iridescent hematite. http://minerals.gps.caltech.edu/manuscripts/in-prep/Submitted/Rainbow_hematite/

Ma C., Gresh J., Rossman G.R., Ulmer G.C., Vicenzi E.P. (2001) Micro-analytical study of the optical properties of rainbow and sheen obsidians. *The Canadian Mineralogist*, Vol. 39, No. 1, pp. 57–71, http://dx.doi.org/10.2113/gscanmin.39.1.57

Ma C., Rossman G.R., Miller J.A. (2007) The origin of color in "fire" obsidian. *The Canadian Mineralogist*, Vol. 45, No. 3, pp. 551–557, http://dx.doi.org/10.2113/gscanmin.45.3.551

Mendes M., Lobato L.M., Kunzmann M., Halverson G.P., Rosière C.A. (2017) Iron isotope and REE+Y composition of the Cauê banded iron formation and related iron ores of the Quadrilátero Ferrífero, Brazil. *Mineralium Deposita*, Vol. 52, No. 2, pp. 159–180, http://dx.doi.org/10.1007/s00126-016-0649-9

Miura Y., Tomisako T. (1978) Ion microprobe mass analysis of exsolution lamellae in labradorite feldspar. *American Mineralogist*, Vol. 63, No. 5-6, pp. 584–590.

Nadin E.S. (2007) The secret lives of minerals. *Engineering and Science*, Vol. 70, No. 1, pp. 10–20.

Niederberger M., Cölfen H. (2006) Oriented attachment and mesocrystals: non-classical crystallization mechanisms based on nanoparticle assembly. *Physical Chemistry Chemical Physics*, Vol. 8, No. 28, pp. 3271–3287, http://dx.doi.org/10.1039/B604589H

Niederberger M., Krumeich F., Hegetschweiler K., Nesper R. (2002) An iron polyolate complex as a precursor for the controlled synthesis of monodispersed iron oxide colloids. *Chemistry of Materials*, Vol. 14, No. 1, pp. 78–82, http://dx.doi.org/10.1021/cm0110472

Ning G., Flemming R.L. (2005) Rietveld refinement of LaB_6: Data from μXRD. *Journal of Applied Crystallography*, Vol. 38, pp. 757–759, http://dx.doi.org/10.1107/S0021889805023344

Ocaña M., Morales M.P., Serna C.J. (1995) The growth mechanism of α-Fe_2O_3 ellipsoidal particles in solution. *Journal of Colloid and Interface Science*, Vol. 171, No. 1, pp. 85–91, http://dx.doi.org/10.1006/jcis.1995.1153

Palache C., Berman H.M., Frondel C. (1944) *The System of Mineralogy of James Dwight Dana and Edward Salisbury Dana*, 7th ed. Wiley, New York.

Penn R.L., Banfield J.F. (1998) Imperfect oriented attachment: dislocation generation in defect-free nanocrystals. *Science*, Vol. 281, No. 5379, pp. 969–971, http://dx.doi.org/10.1126/science.281.5379.969

Posnjak E., Merwin H.E. (1919) The hydrated ferric oxides. *American Journal of Science*, Vol. 47, No. 281, pp. 311–348, http://dx.doi.org/10.2475/ajs.s4-47.281.311

Putnis A. (2002) Mineral replacement reactions: from macroscopic observations to microscopic mechanisms. *Mineralogical Magazine*, Vol. 66, No. 5, pp. 689–708, http://dx.doi.org/10.1180/0026461026650056

Reeves N.J., Mann S. (1991) Influence of inorganic and organic additives on the tailored synthesis of iron oxides. *Journal of the Chemical Society, Faraday Transactions*, Vol. 87, No. 24, pp. 3875–3880, http://dx.doi.org/10.1039/ft9918703875

Rietveld H. (1969) A profile refinement method for nuclear and magnetic structures. *Journal of Applied Crystallography*, Vol. 2, No. 2, pp. 65–71, http://dx.doi.org/10.1107/S0021889869006558

Rosière C.A., Chemale Jr. F. (2008) Brazilian iron formations and their geological setting. *Brazilian Journal of Geology*, Vol. 30, No. 2, pp. 274–278.

Rosière C.A., Rios F.J. (2004) The origin of hematite in high-grade iron ores based on infrared microscopy and fluid inclusion studies: the example of the Conceição mine, Quadrilátero Ferrífero, Brazil. *Economic Geology*, Vol. 99, No. 3, pp. 611–624, http://dx.doi.org/10.2113/gsecongeo.99.3.611

Rosière C.A., Siemes H., Quade H., Brokmeier H.-G., Jansen E.M. (2001) Microstructures, textures and deformation mechanisms in hematite. *Journal of Structural Geology*, Vol. 23, No. 9, pp. 1429–1440, http://dx.doi.org/10.1016/S0191-8141(01)00009-8

Schwertmann U., Fitzpatrick R.W., Taylor R.M., Lewis D.G. (1979) The influence of aluminum on iron oxides. Part II. Preparation and properties of Al-substituted hematites. *Clays and Clay Minerals*, Vol. 27, No. 2, pp. 105–112, http://dx.doi.org/10.1346/CCMN.1979.0270205

Song B., Eom S.C., Shin J.H. (2014) Disorder and broad-angle iridescence from *Morpho*-inspired structures. *Optics Express*, Vol. 22, No. 16, pp. 19386–19400, http://dx.doi.org/10.1364/OE.22.019386

Stanjek H., Schwertmann U. (1992) The influence of aluminum on iron oxides. Part XVI: Hydroxyl and aluminum substitution in synthetic hematites. *Clays and Clay Minerals*, Vol. 40, No. 3, pp. 347–354, http://dx.doi.org/10.1346/CCMN.1992.0400316

Sugimoto T., Khan M.M., Muramatsu A. (1993) Preparation of monodisperse peanut-type α-Fe_2O_3 particles from condensed ferric hydroxide gel. *Colloids and Surfaces A: Physicochemical and Engineering Aspects*, Vol. 70, No. 2, pp. 167–169, http://dx.doi.org/10.1016/0927-7757(93)80285-M

Sugimoto T., Wang Y., Itoh H., Muramatsu A. (1998) Systematic control of size, shape and internal structure of monodisperse α-Fe_2O_3 particles. *Colloids and Surfaces A: Physicochemical and Engineering Aspects*, Vol. 134, No. 3, pp. 265–279, http://dx.doi.org/10.1016/S0927-7757(97)00103-9

Tardy Y., Nahon D. (1985) Geochemistry of laterites, stability of Al-goethite, Al-hematite, and Fe^{3+}-kaolinite in bauxites and ferricretes: an approach to the mechanism of concretion formation. *American Journal of Science*, Vol. 285, No. 10, pp. 865–903.

Toby B.H. (2001) EXPGUI, a graphical user interface for GSAS. *Journal of Applied Crystallography*, Vol. 34, pp. 210–213, http://dx.doi.org/10.1107/S0021889801002242

Torrent J., Schwertmann U., Barrón V. (1994) Phosphate sorption by natural hematites. *European Journal of Soil Science*, Vol. 45, No. 1, pp. 45–51, http://dx.doi.org/10.1111/j.1365-2389.1994.tb00485.x

Vaughan D.J., Tossell J.A., Stanley C.J. (1987) The surface properties of bornite. *Mineralogical Magazine*, Vol. 51, No. 360, pp. 285–293, http://dx.doi.org/10.1180/minmag.1987.051.360.11